Basic research for ultrasound-guided injection into skeletal muscle lesions in an experimental animal model

From Osaka University Graduate School of Medicine, Suita, Japan

Cite this article:
Bone Joint Res 2025;14(1):
33–41.

DOI: 10.1302/2046-3758.
141.BJR-2024-0090.R1

Correspondence should be sent to Takashi Kanamoto
takanamoto2@gmail.com

K. Fujimoto,[1] T. Kanamoto,[1] S. Otani,[1] R. Miyazaki,[1] K. Ebina,[2] K. Nakata[1]

[1]Department of Medicine for Sports and Performing Arts, Osaka University Graduate School of Medicine, Suita, Japan
[2]Department of Musculoskeletal Regenerative Medicine, Osaka University Graduate School of Medicine, Suita, Japan

Aims

Ultrasound-guided injection techniques are expected to enhance therapeutic efficacy for skeletal muscle injuries and disorders, but basic knowledge is lacking. The purpose of this study was to examine the diagnostic accuracy of ultrasound for abnormal skeletal muscle lesions, and to examine the distribution patterns of solution and cells injected into abnormal muscle lesions under ultrasound guidance.

Methods

A cardiotoxin (CTX)-induced muscle injury model was used. Briefly, CTX was injected into tibialis anterior muscle in rats under ultrasound observation. First, the diagnostic accuracy of abnormal muscle lesions on ultrasound was examined by comparing ultrasound findings and histology. Next, Fast Green solution and green fluorescent protein (GFP)-labelled cells were simultaneously injected into the abnormal muscle lesions under ultrasound guidance, and their distribution was evaluated.

Results

Evaluation of short-axis ultrasound images and cross-sectional histological staining showed a strong correlation ($r = 0.927$; $p < 0.001$) between the maximum muscle damage area in ultrasound and haematoxylin and eosin (H&E) staining evaluations. Histological analysis showed that ultrasound-guided injection could successfully deliver Fast Green solution around the myofibres at the site of injury. In contrast, the distribution of injected cells was very localized compared to the area stained with Fast Green.

Conclusion

This experimental animal study demonstrated the potential of ultrasound to quantitatively visualize abnormalities of skeletal muscle. It also showed that ultrasound-guided injections allowed for highly accurate distribution of solution and cells in abnormal muscle tissue, but the patterns of solution and cell distribution were markedly different. Although future studies using a more clinically relevant model are necessary, these results are important findings when considering biological therapies for skeletal muscle injuries and disorders.

Article focus

- Ultrasound-guided injection techniques are expected to enhance therapeutic efficacy for skeletal muscle injuries and disorders, but basic knowledge is still lacking.

Key messages

- Ultrasonographic and histological evaluations have high correlation with regard to quantification of the abnormal muscle tissue lesions.
- Histological analysis showed that ultrasound-guided injection could successfully deliver solution and cells in abnormal muscle tissue, but the patterns of solution

and cell distribution were markedly different.

Strengths and limitations

- Ultrasound-guided intervention employing clinically used devices was performed on the in vivo model.
- This study used the cardiotoxin (CTX)-induced muscle injury model, a model which is frequently used but differs from clinical practice.

Introduction

Skeletal muscle injuries and disorders are basically diagnosed on history and physical examination, and in many cases imaging studies, including ultrasound, provide important information. Ultrasound-guided interventions, such as biopsy, aspiration, and infusion of drugs, are extremely important procedures in many areas of clinical medicine.[1] Ultrasound-based diagnosis of skeletal muscle disorders has been reported to be comparable to that of MRI in the prognosis of indirect traumatic muscle injury, and may also be used to diagnose neuromuscular disorders.[2,3] Although it is known that high-resolution ultrasound images reflect normal skeletal muscle tissue well, relatively few reports have examined how ultrasound images reflect abnormal muscle tissue.[2,4,5] In particular, few studies have used histological findings as the gold standard, and studies focusing on skeletal muscle injuries and disorders are extremely limited.[6-9]

In recent years, much basic and translational research has focused on biological therapies for various skeletal muscle disorders, including traumatic skeletal muscle injuries, neuromuscular diseases with spasticity, and muscle atrophy.[10-14] Local administration via intramuscular injection has been recognized as a particularly useful method for localized disease owing to its safety and local residence time.[15] Although several animal studies and human clinical trials have been designed and conducted to evaluate various aspects of this technique,[16] there is no consensus on the administration protocols, including drug dose, cell numbers, injection site, or frequency of injection. In the case of intramuscular injections into skeletal muscle tissue, which has dense connective tissue, the distribution of the injected substance is expected to be affected by the properties of the injected substance and the condition of the injection site; however, there is insufficient knowledge in this area.[15,17]

We hypothesized that there would be histological findings corresponding to ultrasonographic findings of skeletal muscle injuries and disorders, and that ultrasound would allow quantitative assessment of the area of muscle injury. We also hypothesized that solutions and cells injected into injured muscle tissue would show different distribution patterns. To investigate these hypotheses, we used the rat cardiotoxin (CTX)-induced muscle injury model, which is frequently used as a highly reproducible model of muscle injury. This experimental animal study was designed to explore the following: to compare the largest damaged muscle area between ultrasound evaluation and histological haematoxylin and eosin (H&E) staining after determining the inter- and intraobserver accuracy histological and ultrasound evaluations; and to evaluate the distribution of solutions and cells injected under ultrasound guidance. Although there are some issues, such as differences in muscle tissue size and composition, which affect ultrasound evaluation when compared to actual human muscle injury, the results obtained are expected to provide basic data for conducting human clinical studies.

Methods

Animals

This research has been approved by the institutional review board (IRB) of the authors' affiliated institution. All the animal experiments in this study adhered to the ARRIVE guidelines, and an ARRIVE checklist is included in the Supplementary Material to show this. A total of 30 male Wistar Hannover rats (Nihon Clea, Japan) aged eight to 13 weeks were used in the experiments. CAG-EGFP rats were purchased from Japan SLC (Japan). The rats were housed (two per cage) in a temperature-controlled room with a 12-hour day/night cycle, and an adequate amount of food and water was provided ad libitum. A mixture of three agents was administered intraperitoneally to achieve analgesia and sedation: medetomidine (Domitor; Nippon Zenyaku Kogyo, Japan) 0.3 mg/kg; midazolam (Dormicum; Maruishi Pharmaceutical, Japan) 4.0 mg/kg; and butorphanol (Vetorphale; Meiji Seika Pharma, Japan) 5.0 mg/kg.

Study design and sample size

In this study, muscle lesions were created on only one lower limb of the animals. Inter- and intraobserver intraclass correlation coefficient (ICC) in histological and ultrasonographic evaluations was performed on ten tibialis lesions created in the anterior muscle used for the study. Quantitative comparison of abnormal lesions in ultrasound images and H&E staining was performed using lesions created in 12 tibialis anterior muscles. Comparison of solution and cell distribution immediately after injection was performed using lesions created in five tibialis anterior muscles. A total of 30 rats were used in this study. In addition to the animals used for the aforementioned measurements (17 rats), six rats were used for establishing the ultrasound-guided injection technique, six rats for examining histological findings, and one rat for collecting adipose-derived cells.

Ultrasound examination

The rats were evaluated in B (brightness) mode using SONIMAGE HS1 ultrasound system with a linear probe HL18-4 (10 MHz) (Konica Minolta, Japan). The spatial resolution of this system was 0.13 mm or less (distance direction), 0.3 mm or less (azimuth direction). Prior to ultrasound examination, the tibialis anterior (TA) muscle was delineated by placing the rat in a supine, fixed position with the knee and ankle joints in extension, and the body hair on the lower limb of the rat was removed. Short-axis ultrasound images were acquired as perpendicular to the muscle fibres as possible, using echogenicity as a cue. To obtain a long-axis image, the probe was manipulated with care to make the beam parallel to the muscle fibres.

Generation of skeletal muscle injury model by ultrasound-guided CTX injection

Needles of 25 G (SGE, Australia) or 30 G (Termo Co., Japan) diameter were inserted in the centre of the long and short axes of the TA muscle, and 25 to 150 µl of 10 µM CTX

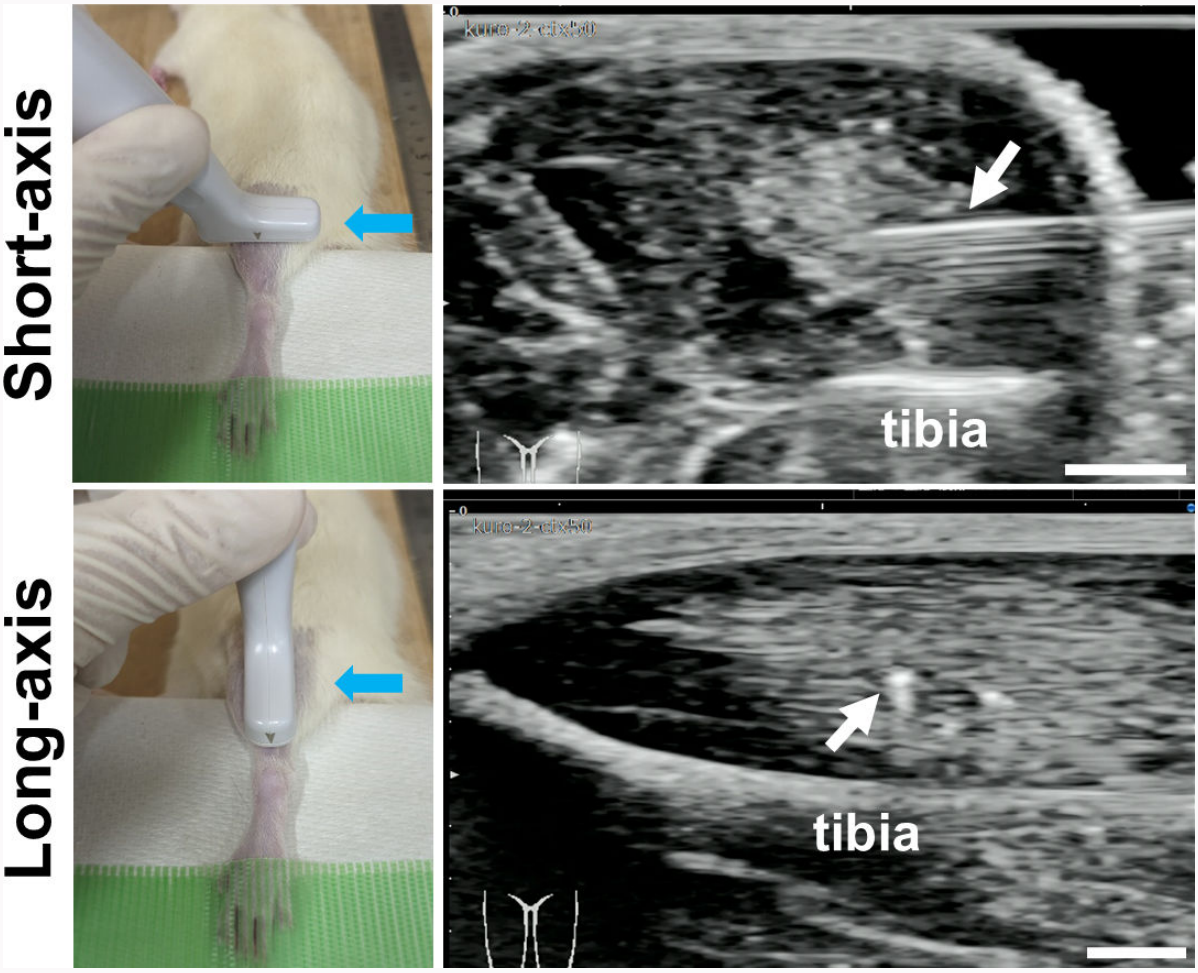

Fig. 1
Ultrasound-guided cardiotoxin injection into rat tibialis anterior muscle. In the macroscopic photographs, probe positions during long-axis/short-axis imaging are shown. Blue arrows indicate the direction of needle puncture. In the ultrasound images, positions of the needle in the muscle tissue are indicated with white arrows. Scale bars = 2 mm.

(Latoxan, France) was injected under ultrasound observation using long-axis in-plane techniques (25 µl for one rat, 50 µl for nine rats, and 150 µl for two rats). To measure the lesion size, still images with the largest damaged area were selected by checking the stored short-axis video image frame-by-frame. The standard video frame rate was 15 frames per second.

Ultrasound-guided drug/cell injection into the injured muscle lesion

Animals were used 24 hours after injection of 100 µl of 10 µM CTX. Adipose-derived cells were isolated from a CAG-EGFP rat using a standard collagenase digestion. Cells at passage 2 were prepared with Fast Green solution (0.2%). A needle tip was placed in the lesion under ultrasound guidance, and 100 µl (1×10^6 cells) of cell suspension was injected. Within 30 minutes after injection, the TA muscle was harvested. The measurements of the distribution area of Fast Green and GFP-positive cells were performed using same sections. Picrosirius red (PSR) staining and immunostaining were performed using serial sections.

Preparation of frozen tissue sections

The rats were euthanized by exsanguination following deep anaesthesia with isoflurane, and the TA muscle was harvested. After skin and fascia incisions, the distal tendon was cut and collected as a single mass to avoid damaging the muscle tissue. The TA muscle was quick-frozen using isopentane cooled with liquid nitrogen and stored at -80°C. A cryostat (CM1860; Leica) was used for preparation of 10 µm frozen sections. Careful attention was paid to obtain cross-sections perpendicular to the long axis of the tibialis anterior muscle.

H&E and PSR staining

H&E staining, which is frequently used for histological evaluation of skeletal muscle morphology, and PSR staining, which is excellent for depicting collagen fibres, were used. TA sections were washed in phosphate-buffered saline (PBS) for five minutes and then stained using H&E solutions and PSR solution according to the manufacturer's standard protocol (Muto Pure Chemicals, Japan). In the cross-section, it was observed that the TA muscle was separated from the extensor digitorum longus muscle by fascia (Supplementary Figure a).

Immunostaining

Anti-type I collagen, anti-F4/80 antibody, anti-laminin antibody, fluorescent phalloidin, and 4',6-diamidino-2-phenylindole (DAPI) were used to delineate

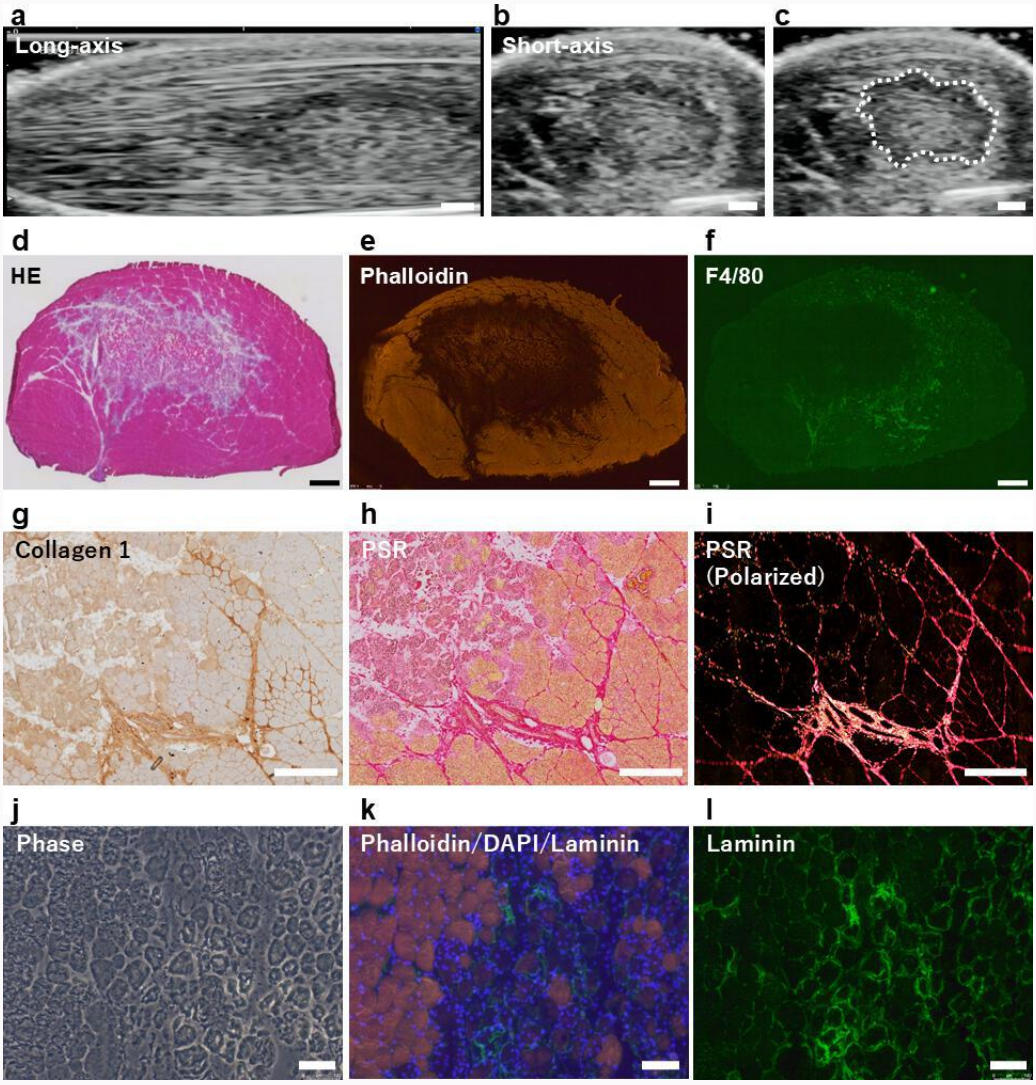

Fig. 2

Ultrasound images and histological sections of tibialis anterior 24 hours after cardiotoxin (CTX) injection. a) Long-axis and b) short-axis ultrasound images. c) In a short-axis ultrasound image, lesion containing more hypoechoic area than normal muscle tissue is outlined with a dotted line. d) to i) Histological analysis performed using the cross-sectional sections. Staining with haematoxylin and eosin (HE), phalloidin, and anti-F4/80 antibody is shown. g) to l) Stained images of the area bordering CTX-induced muscle injury and surrounding tissue. Myofibres, endomysium, and perimysium at the site of muscle injury were stained with anti-collagen 1 antibody, Picrosirius red (PSR) without/with polarized microscopy, anti-laminin antibody, phalloidin, and 4′,6-diamidino-2-phenylindole (DAPI). In the merged image, myofibres were labelled with phalloidin (red), nuclei with DAPI (blue), and endomysium with laminin (green). Scale bars = 1 mm in a) to f), 500 μm in g) to i), and 100 μm in j) to l).

collagen fibres, macrophages, endomysium, and muscle fibres, respectively. After blocking with Blocking One Histo (06349-64; Nacalai Tesque Inc., Japan) in 1× PBST (1× PBS, 0.1% Tween 20) at room temperature for one hour, the sections were incubated at 4°C overnight with the following primary antibodies: goat anti-type I collagen (1:200; 1310-01; SouthernBiotech, USA), rat anti-F4/80 (1:200; ab6640; Abcam, UK), and rabbit anti-laminin (1:200; ab11575; Abcam). For anti-type I collagen, the immune complexes were detected using anti-goat IgG H&L (HRP) (1:500; ab97110; Abcam) and ImmPACT DAB (SK-4105; Vector Laboratories, USA). For anti-F4/80 and anti-laminin, the immune complexes were detected using anti-rat IgG (H + L) Alexa Fluor 594 (1:400; A-21209; Invitrogen, Thermo Fisher Scientific, USA) or anti-rabbit IgG (H + L) Alexa Fluor 488 (1:400; A-21206; Invitrogen) antibodies. The actin cytoskeleton was visualized using Acti-stain 555 Fluorescent phalloidin (PHDH1; Cytoskeleton, USA). Images were obtained using a DMi8 (Leica Microsystems, Germany) microscope or an Olympus BX53 microscope (Olympus, Japan).

Quantitative evaluations

All quantitative evaluations in this study were performed using short-axis ultrasound and histological images of the tibialis anterior muscle. For histological measurements, H&E staining images, which are frequently used to evaluate CTX-induced muscle lesions, were evaluated. To evaluate the distribution of Fast Green and GFP-positive cells, bright-field and fluorescence images were acquired without additional staining. The blue-stained regions (as the distribution of injected Fast Green solution) and fluorescent regions (as the distribution of injected cells) were measured, respectively. The region of interest (ROI) was determined using the hand tool func-

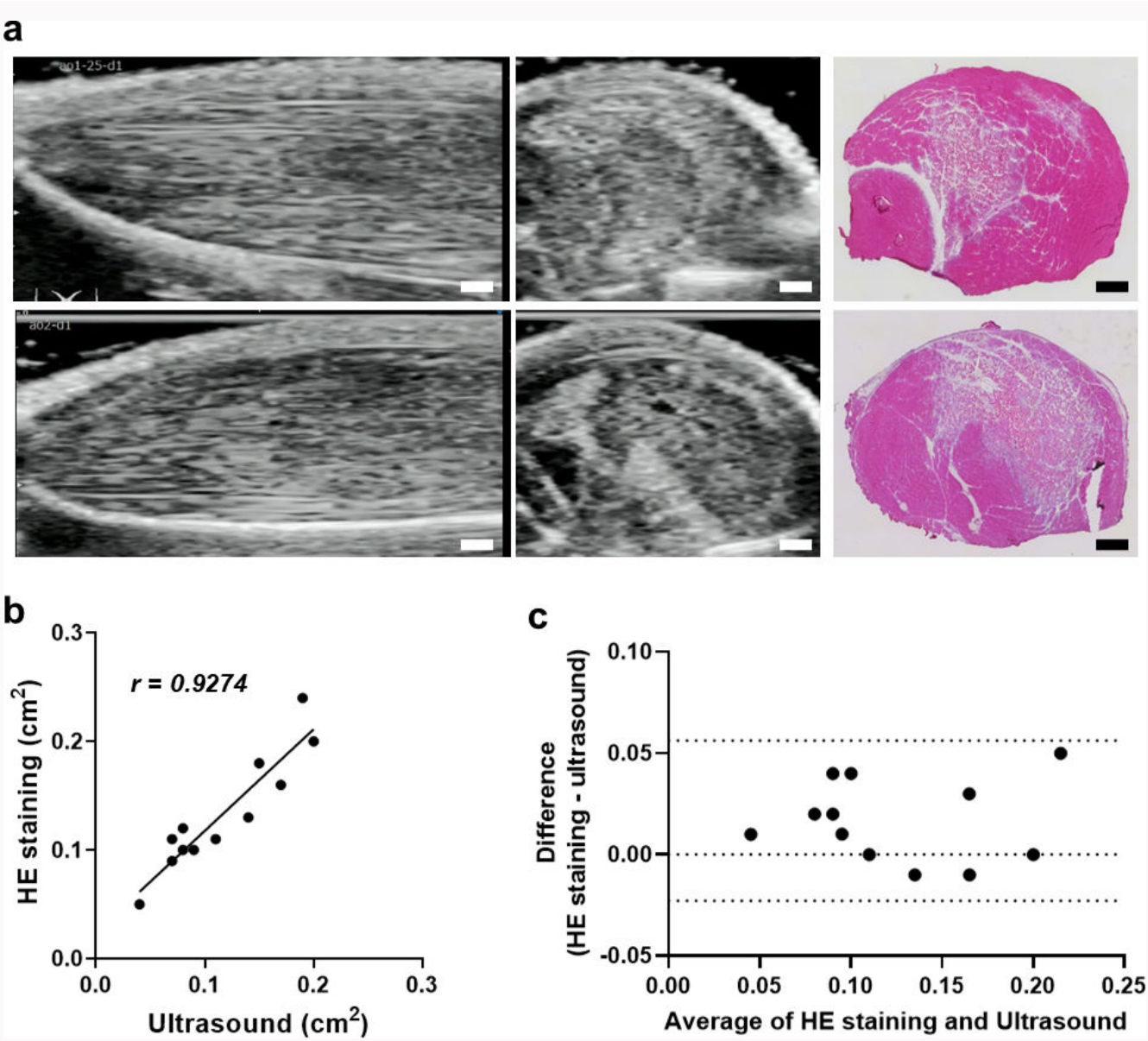

Fig. 3
Quantitative comparison between ultrasound and histological measurements of muscle injury area. a) Typical ultrasound images and cross-sectional haematoxylin and eosin (HE) staining of tibialis anterior 24 hours after cardiotoxin (CTX) injection. b) The comparison of skeletal muscle injury areas measured in ultrasound and HE-stained images. c) Bland-Altman plot of the differences (y-axis) and means (x-axis) of the muscle injury areas measured by HE staining and ultrasound (n = 12). Scale bars = 1 mm.

Table I. Inter- and intraobserver intraclass correlation coefficient in histological and ultrasonographic evaluations.

	Intraobserver		Interobserver	
Variable	**ICC (1,1)**	**95% CI**	**ICC (2,1)**	**95% CI**
Ultrasound evaluation	0.9743	0.9062 to 0.9935	0.9724	0.8995 to 0.993
Histological measure-ment	0.9803	0.9324 to 0.9946	0.9822	0.9353 to 0.9952

ICC, intraclass correlation coefficient.

tion of Lenaraf 220b software (Vector Japan, Japan) and was quantitatively measured.

Intra- and interobserver reproducibility

Two examiners (TK and SO, two orthopaedic surgeons experienced in musculoskeletal ultrasound measurements) independently performed histological and ultrasound assessments on randomly selected and blinded CTX-induced lesions (11 lesions for histology, ten lesions for ultrasound). The trials were performed on two different days and analyzed independently by two observers (TK and SO). Both intra- and interobserver reliability rates were assessed using ICC.

Statistical analysis

The relationship between ultrasound and H&E staining for quantitative assessment of the area of muscle damage

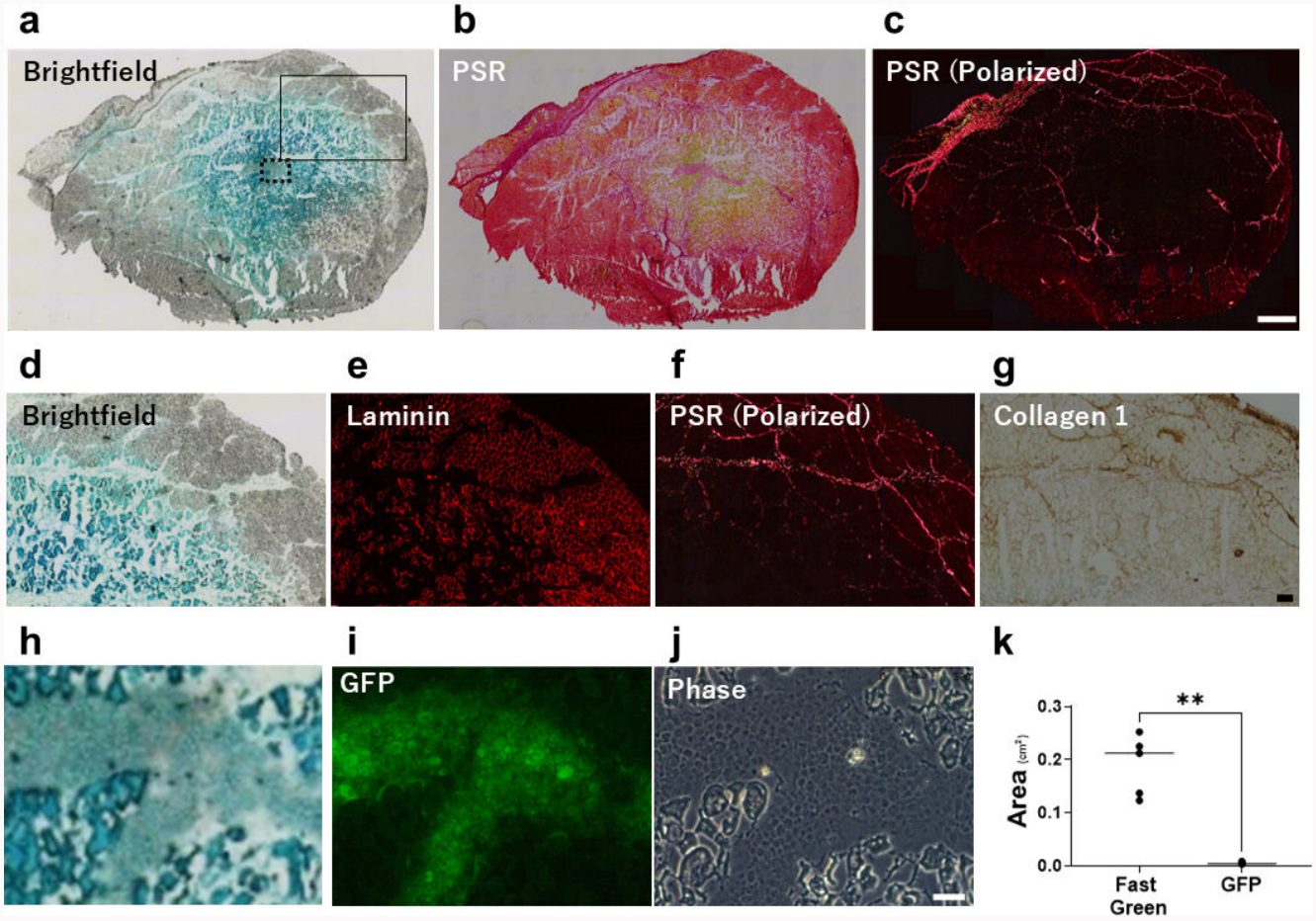

Fig. 4

The distribution of the injected solution and cells. a) to j) Images of cryosections immediately created after injection. a) Brightfield image. b) and c) Images of staining with Picrosirius red (PSR). d) to g) Images of area indicated by solid line in panel a). d) Brightfield image. e) Image of staining with anti-laminin antibody. f) Image of staining with PSR. g) Image of staining with anti-collagen 1 antibody. h) to j) Images of area indicated by dotted line in panel a). h) Brightfield image. i) GFP-positive cells. j) Image of phase contrast. k) Graph showing a comparison between Fast Green-stained and GFP-positive areas. Scale bars = 1 mm for upper panels, 200 μm for middle panels, and 100 μm for lower panels.

was investigated using Pearson correlation coefficient and Bland-Altman plots. Both intra- and interobserver reliabilities were assessed using ICC. Analyses were performed using GraphPad Prism 9.0.0 (GraphPad Software, USA) or Ekuseru-Toukei (Social Survey Research Information Co., Ltd., Japan). Data are presented as mean (SD), and statistical significance was set at $p < 0.05$.

Results

Ultrasound-guided CTX injection into rat tibialis anterior muscle

The rat TA muscle was reproducibly delineated along the long and short axes (Figure 1). Using short axis out-of-plane and long-axis in-plane techniques, CTX was injected into the muscle belly near the centre of the long axis of the TA muscle while confirming the needle tip position in the ultrasound image. The muscle tissue injected with the drug solution became more hyperechoic than the surrounding tissue.

Histological analysis of lesions with abnormal patterns in ultrasound images

Ultrasound images obtained 24 hours after CTX injection showed areas with lower echogenicity than healthy muscle fibres in both the short- and long-axis images (Figures 2a to 2c). Haematoxylin and eosin (H&E) staining of the samples prepared following the ultrasound observations revealed damaged areas with reduced eosin staining (Figure 2d), absence of phalloidin-stained myofibres in some areas (Figure 2e), and expression of macrophage markers in some areas (Figure 2). Collagen 1 staining signal was reduced in the injured region (Figure 2g), and PSR-stained perimysium was fragmented (Figures 2h and 2i). In the injured area, muscle fibres showing morphological changes were observed (Figure 2j). These abnormally shaped muscle fibres showed decreased expression of phalloidin (Figure 2k), but not of laminin, which indicates endomysium (basal lamina) (Figure 2l).

Quantitative comparison of abnormal lesions in ultrasound images and H&E staining

Various sizes of muscle lesions were observed as a result of injecting different volumes of CTX solution at the same concentration (Figure 3a, Supplementary Figures b and c). Evaluation of short-axis ultrasound images and cross-sectional histological staining showed a strong correlation ($r = 0.927$; $p < 0.001$) between the maximum muscle damage area in ultrasound and H&E staining evaluations (Figure 3b).

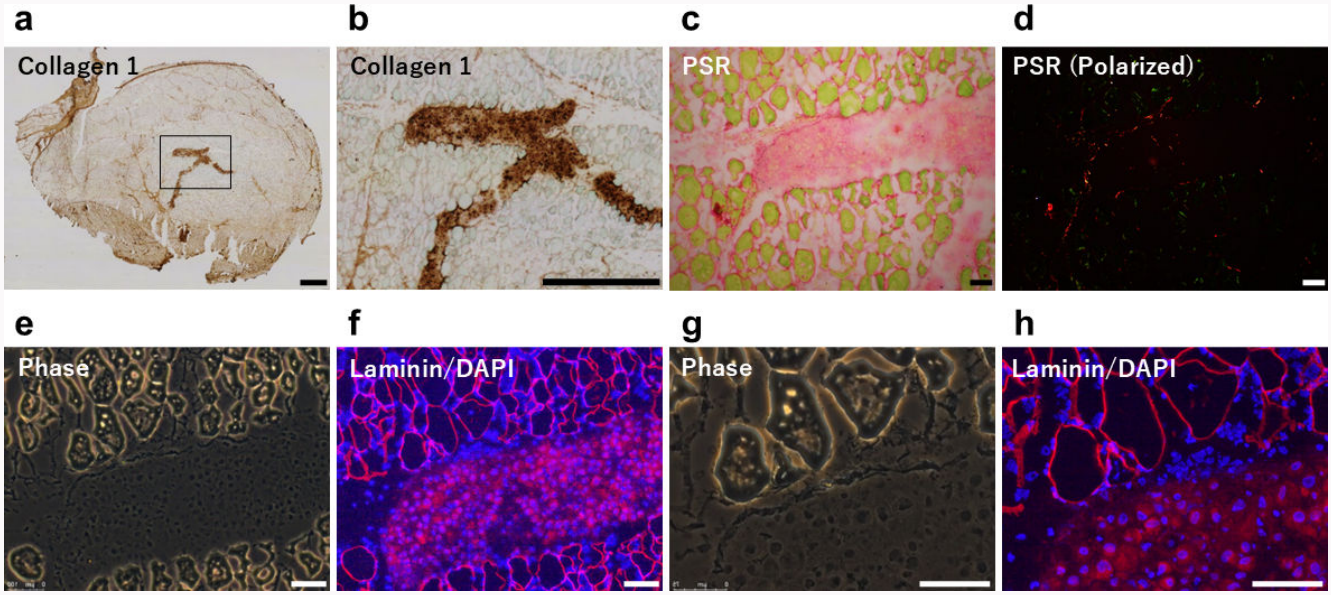

Fig. 5
The relationship between muscle membranes and distribution of injected cells. a) and b) Images of staining with anti-collagen 1 antibody. Solid line in panel a) indicates area shown in panel b). The cells were distributed in a pattern along the perimysium. c) to h) Images of injected cells in injured muscle tissue. c) and d) Images of staining with Picrosirius red. Fragmented red signals were observed at the margins of the cell aggregates. e) to h) The merged images labelled with laminin (red) and nuclei with 4′,6-diamidino-2-phenylindole (DAPI) (blue). No clear contact between the laminin staining and cell aggregates was observed. Scale bars = 100 μm.

Ultrasound measurements were significantly lower (mean 86% (SD 14)) than histological measurements (Figure 3c). Both intra- and interobserver reproducibility of the quantitative assessment of the muscle injury area by ultrasound imaging and histological analysis were sufficiently high (Table I).

Distribution of solution injected under ultrasound guidance into CTX-induced skeletal muscle injury lesions

During ultrasound-guided injection of Fast Green solution into muscle lesions 24 hours after CTX injection, an increase in the muscle tissue cross-sectional area was observed (Supplementary Video 1). Tissue samples prepared immediately after the injection showed wide distribution of the Fast Green stain in the muscle injury lesions (Figures 4a, 4d, and 4h). PSR staining signal was absent or fragmented (Figures 4b, 4c, and 4f), and laminin staining signal was discontinuous (Figure 4e) in Fast Green-stained areas. In contrast, strong PSR staining signal with continuity and anti-collagen 1 antibody signal were observed in areas lacking Fast Green staining (Figures 4b, 4c, 4f, and 4g).

Distribution of cells injected under ultrasound guidance into CTX-induced skeletal muscle injury lesions

The distribution of cells injected into the area of muscle injury was localized to 2.7% ± 0.9% of the Fast Green solution distribution area (Figures 4h to 4k). The cells were distributed in a pattern along the perimysium, and fragmented PSR staining was observed at the margins of the cell aggregates (Figures 5a to 5d, 5e, and 5g). No contact between the laminin staining and cell aggregates was observed (Figures 5f and 5h).

Discussion

In this study, the quantitative assessment of the muscle injury area by ultrasound imaging and histological analysis was sufficiently reproducible. The evaluation of short-axis ultrasound images and cross-sectional histological staining showed a strong correlation between the maximum muscle damage area in ultrasound and H&E staining evaluations. It also showed that ultrasound-guided injections allowed for highly accurate distribution of solution and cells in abnormal muscle tissue, but the patterns of solution and cell distribution were markedly different.

Although studies using animal muscle injury models have been reported previously, including one that compared ultrasound and histological evaluation of muscle tissue using mepivacaine-injected rats, and another that demonstrated the relationship between the ratio of fibrous tissue and echo intensity in canine muscle specimens,[2,6] quantitative evaluation of the muscle tissue has not been fully established, and several unresolved issues remain. In addition, muscle injuries are often detected in ultrasound images in clinical scenarios,[3] but to the best of our knowledge there are no reports comparing them to histological findings. Although further studies are needed to generalize the results of this study, they highlight the utility of ultrasound imaging in skeletal muscle injuries and disorders. Muscle thickness and cross-sectional area are commonly used to quantitatively evaluate ultrasound images of skeletal muscles.[18] In the present study, we quantified the muscle damage area using a method with high inter-rater reliability, and demonstrated a strong correlation between ultrasound and histological assessments. Although assessment of the size of space-occupying lesions in the liver and breast tissue has been found to be of high value,[19,20] there have been few attempts to assess the extent of skeletal muscle damage.[3]

Ultrasound-guided interventions are frequently used in clinical practice for local anaesthesia, nerve blocks for pain treatment, and aspiration of haematomas and abscesses, and

greatly enhance the accuracy of the approach to the target tissue.[21] In the present study, histological evaluation confirmed that ultrasound-guided injection allowed for precise distribution of the solution and cells to the site of muscle injury, thus providing new evidence for the utility of ultrasound-guided intervention.[22] In addition, the clear differences in ultrasound images based on the injection site (healthy or damaged tissue) demonstrate the importance of using ultrasound imaging to inject drugs precisely into lesions in clinical practice. The results of this study strongly suggest that the structure of the muscle tissue, particularly the condition of the endomysium and perimysium, is an important factor in solution and cell distribution. With regard to distribution within the tissue, the molecular size and affinity of the injected drug solution would also be a crucial factor. In this study, only the Fast Green solution prepared in PBS was examined, and further studies using multiple drug solutions are needed. Studies on intramuscular cells in X-linked muscular dystrophy (MDX) mice, CTX-induced injured muscle tissue, and transplantation studies in patients with DMD and healthy primates have all reported few viable cells and their localization,[15,23] indicating that the site and technique of muscle transplantation are important.

This study has several limitations. First, as a CTX-induced muscle injury model was used for the ultrasound imaging studies, the intramuscular injection model is not identical to actual muscle disease or skeletal muscle injury. Future studies using a more clinically relevant model are necessary. Furthermore, the differences in muscle size and muscle and connective tissue composition between rodent and human muscle tissue may also affect ultrasound imaging and distribution of administered material. A second important limitation is that both the ultrasound images and distribution of the solution and cells in the muscle tissue following intramuscular injections were evaluated cross-sectionally; further studies are warranted to evaluate longitudinal sections, which may provide clinically meaningful findings. Moreover, in the present study all quantitative evaluations were performed using only short-axis ultrasound and histological images of the tibialis anterior. Naturally, 3D evaluation and both long-axis and short-axis evaluation are desirable in order to evaluate 3D structures. However, in ultrasound images of skeletal muscle, it is difficult to distinguish lesions from healthy areas in long-axis images compared to short-axis images, where it is easier to obtain images perpendicular to the muscle fibres. The possibility of quantitative evaluation of injured muscle lesions by ultrasound, as demonstrated in this study, is currently limited.

In conclusion, short-axis ultrasound images and cross-sectional histological staining showed a strong correlation with regard to quantitative assessment of damaged muscle tissue in this CTX-induced muscle injury model. In addition, ultrasound-guided injections were shown to provide accurate delivery of solutions and cells in abnormal muscle tissue. The distribution patterns of solutions and cells injected into damaged muscle tissue were markedly different and highly dependent on the condition of the myofibres and muscle membrane. The results of this study are expected to provide essential knowledge for diagnosis and therapeutic interventions in skeletal muscle injuries and disorders using ultrasound.

Supplementary material

Figures showing the anatomical information of histological images and quantitative measurements of muscle injury areas. A video is also included showing the ultrasound-guided solution injection into the cardiotoxin-induced muscle lesion. An ARRIVE checklist is included to show that the ARRIVE guidelines were adhered to in this study.

References

1. **Louis LJ**. Musculoskeletal ultrasound intervention: principles and advances. *Radiol Clin North Am*. 2008;46(3):515–533.
2. **Pillen S**, **van Alfen N**. Skeletal muscle ultrasound. *Neurol Res*. 2011; 33(10):1016–1024.
3. **Ossola C**, **Curti M**, **Calvi M**, **et al**. Role of ultrasound and magnetic resonance imaging in the prognosis and classification of muscle injuries in professional football players: correlation between imaging and return to sport time. *Radiol Med*. 2021;126(11):1460–1467.
4. **Turner NJ**, **Badylak SF**. Regeneration of skeletal muscle. *Cell Tissue Res*. 2012;347(3):759–774.
5. **Barbosa FDS**, **Nascimento BSS**, **Silva MCFS**, **Cerqueira TCF**, **de Santana Filho VJ**. Impact of muscle changes assessed by ultrasonography on muscle strength and functioning after ICU discharge: a systematic review with meta-analysis. *Int J Environ Res Public Health*. 2024;21(7):908.
6. **Jiménez-Díaz F**, **Jimena I**, **Luque E**, **et al**. Experimental muscle injury: correlation between ultrasound and histological findings. *Muscle Nerve*. 2012;45(5):705–712.
7. **Leiva-Cepas F**, **Benito-Ysamat A**, **Jimena I**, **et al**. Ultrasonographic and histological correlation after experimental reconstruction of a volumetric muscle loss injury with adipose tissue. *Int J Mol Sci*. 2021;22(13):6689.
8. **Zhou X**, **Wang C**, **Qiu S**, **Mao L**, **Chen F**, **Chen S**. Non-invasive assessment of changes in muscle injury by ultrasound shear wave elastography: an experimental study in contusion model. *Ultrasound Med Biol*. 2018;44(12):2759–2767.
9. **Zhao J**, **Huang H**, **Xu Q**, **Pan Q**, **Guo J**. Quantitative assessment of changes in skeletal muscle injury by computer-aided analysis based on two-dimensional ultrasonography combined with contrast-enhanced ultrasonography and estimated by a modified semi-quantitative scoring system: an experimental study in a contusion model. *Int J Exp Pathol*. 2022;103(5):208–218.
10. **Gharaibeh B**, **Chun-Lansinger Y**, **Hagen T**, **et al**. Biological approaches to improve skeletal muscle healing after injury and disease. *Birth Defects Res C Embryo Today*. 2012;96(1):82–94.
11. **Darabi R**, **Pan W**, **Bosnakovski D**, **Baik J**, **Kyba M**, **Perlingeiro RCR**. Functional myogenic engraftment from mouse iPS cells. *Stem Cell Rev Rep*. 2011;7(4):948–957.
12. **Sharova AA**. Comparison of different consensuses of BTXA in different countries. *J Cosmet Dermatol*. 2016;15(4):540–548.
13. **Raciti L**, **Raciti G**, **Ammendolia A**, **de Sire A**, **Onesta MP**, **Calabrò RS**. Improving spasticity by using botulin toxin: an overview focusing on combined approaches. *Brain Sci*. 2024;14(7):631.
14. **Symington FW**, **Santos EB**. Lysis of human keratinocytes by allogeneic HLA class I-specific cytotoxic T cells. Keratinocyte ICAM-1 (CD54) and T cell LFA-1 (CD11a/CD18) mediate enhanced lysis of IFN-gamma-treated keratinocytes. *J Immunol*. 1991;146(7):2169–2175.
15. **Skuk D**, **Goulet M**, **Tremblay JP**. Intramuscular transplantation of myogenic cells in primates: importance of needle size, cell number, and injection volume. *Cell Transplant*. 2014;23(1):13–25.
16. **Qazi TH**, **Duda GN**, **Ort MJ**, **Perka C**, **Geissler S**, **Winkler T**. Cell therapy to improve regeneration of skeletal muscle injuries. *J Cachexia Sarcopenia Muscle*. 2019;10(3):501–516.
17. **Richard P-L**, **Gosselin C**, **Laliberté T**, **et al**. A first semimanual device for clinical intramuscular repetitive cell injections. *Cell Transplant*. 2010;19(1): 67–78.
18. **Annetta MG**, **Pittiruti M**, **Silvestri D**, **et al**. Ultrasound assessment of rectus femoris and anterior tibialis muscles in young trauma patients. *Ann Intensive Care*. 2017;7(1):104.
19. **Forner A**, **Reig M**, **Bruix J**. Hepatocellular carcinoma. *Lancet*. 2018; 391(10127):1301–1314.

20. **Elmore JG**, **Armstrong K**, **Lehman CD**, **Fletcher SW**. Screening for breast cancer. *JAMA*. 2005;293(10):1245–1256.
21. **del Cura JL**. Ultrasound-guided therapeutic procedures in the musculoskeletal system. *Curr Probl Diagn Radiol*. 2008;37(5):203–218.
22. **Trunz LM**, **Landy JE**, **Dodson CC**, **Cohen SB**, **Zoga AC**, **Roedl JB**. Effectiveness of hematoma aspiration and platelet-rich plasma muscle injections for the treatment of hamstring strains in athletes. *Med Sci Sports Exerc*. 2022;54(1):12–17.
23. **Hamidian Jahromi S**, **Davies JE**. Concise review: skeletal muscle as a delivery route for mesenchymal stromal cells. *Stem Cells Transl Med*. 2019;8(5):456–465.

Author information

K. Fujimoto, Master's degree, Graduate student
T. Kanamoto, MD, PhD, Researcher, Orthopaedic Surgeon
S. Otani, MD, PhD, Orthopaedic Surgeon
R. Miyazaki, MD, Orthopaedic Surgeon
K. Nakata, MD, PhD, Orthopaedic Surgeon, Researcher, Head of Department
Department of Medicine for Sports and Performing Arts, Osaka University Graduate School of Medicine, Suita, Japan.

K. Ebina, MD, PhD, Orthopaedic Surgeon, Researcher, Department of Musculoskeletal Regenerative Medicine, Osaka University Graduate School of Medicine, Suita, Japan.

Author contributions

K. Fujimoto: Data curation, Formal analysis, Investigation, Methodology, Writing – original draft.
T. Kanamoto: Conceptualization, Data curation, Formal analysis, Funding acquisition, Investigation, Methodology, Writing – original draft, Writing – review & editing.
S. Otani: Investigation, Writing – review & editing.
R. Miyazaki: Investigation, Methodology, Writing – review & editing.
K. Ebina: Supervision, Writing – review & editing.
K. Nakata: Conceptualization, Funding acquisition, Supervision, Writing – review & editing.

K. Fujimoto and T. Kanamoto contributed equally to this work.

Funding statement

The authors disclose receipt of the following financial or material support for the research, authorship, and/or publication of this article: this work was supported by the Grants-in-Aid for Scientific Research of the Japan Society for the Promotion of Science, Grant Number # JP 20K11360 and # JP 22K19751, as reported by T. Kanamoto and K. Nakata, respectively.

ICMJE COI statement

T. Kanamoto and K. Nakata report funding from the Grants-in-Aid for Scientific Research of the Japan Society for the Promotion of Science, Grant Number # JP 20K11360 and # JP 22K19751, respectively, related to this study.

Data sharing

The data that support the findings for this study are available to other researchers from the corresponding author upon reasonable request.

Acknowledgements

The authors would like to thank Editage (www.editage.jp) for English language editing.

Ethical review statement

All animal experiments were approved by the Animal Experiment Committee of Osaka University Graduate School of Medicine (approval No.: 04-003-001).

Open access funding

The authors report that the open access funding for their manuscript was self-funded.